2. Hydrodynamic simulation of synchronized oscillatory flows in two coupled collapsible tubes

Y. Araya, H. Ito, and H. Kitahata, Chiba univ.

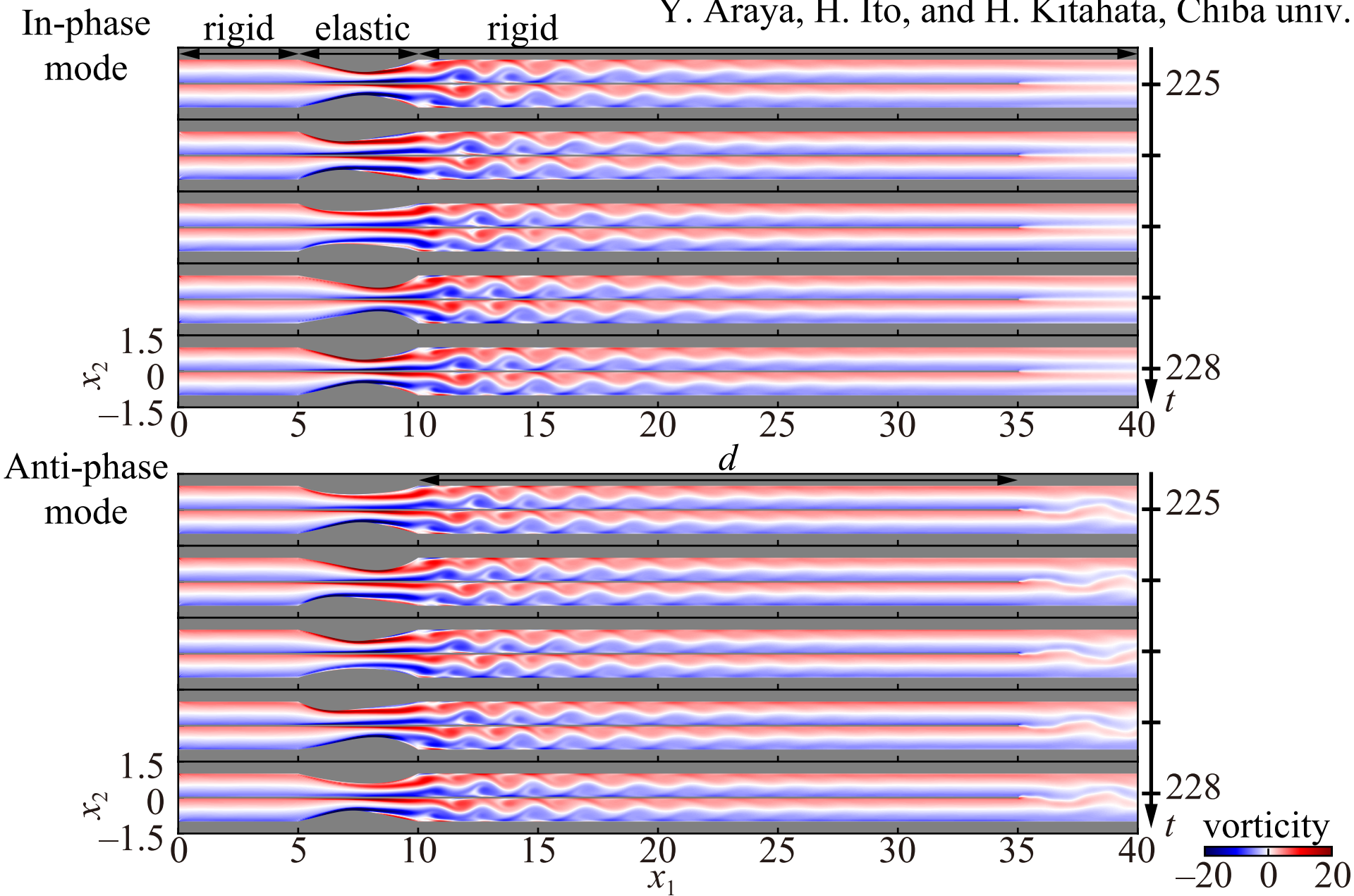

2. Hydrodynamic simulation of synchronized oscillatory flows in two coupled collapsible tubes

Subcritical pitchfork bifurcation
discussed using
only the phase difference

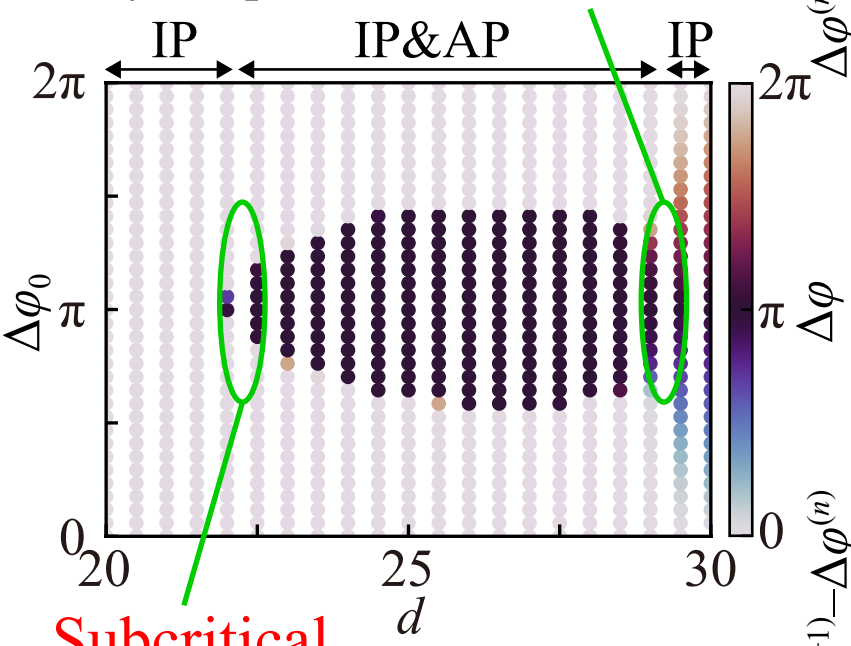

Subcritical Neimark-Sacker bifurcation
discussed using both the phase difference and amplitude

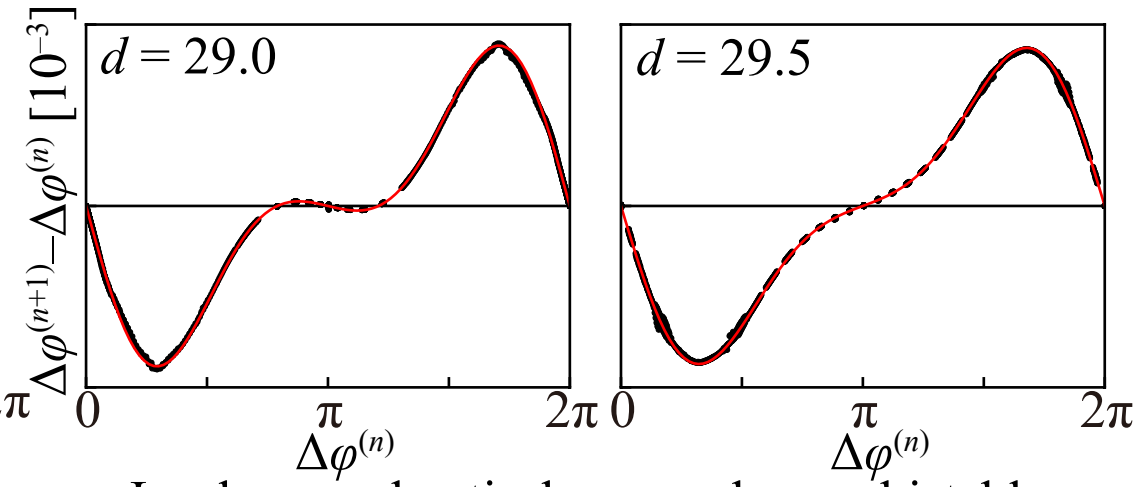

In-phase and anti-phase modes are bistable for middle d.
We clarify the bifurcation structure at two bifurcation points where the stability of anti-phase mode changed.

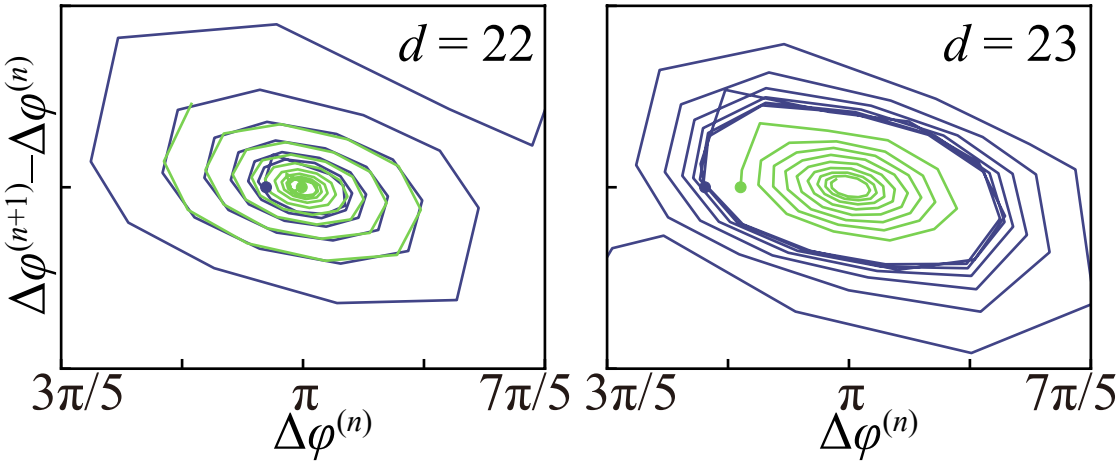

Y. Araya, H. Ito, and H. Kitahata, *Phys. Rev. E* **109**, 054201 (2024).

Dynamics Days Asia Pacific 13 / YKIS2024
Yukawa Institute for Theoretical Physics, Kyoto University, Japan
July 1st — 5th, 2024

Symmetry and dynamics universality in quantum chaos

Ping Fang 方萍
pingfang@bupt.edu.cn

北京郵電大學
Beijing University of Posts and Telecommunications

Symmetry and dynamics universality in quantum chaos

- Model: Quantum kicked rotors with or without time-reversal symmetry

- Dynamics is universal, determined only by the system's symmetry, both for the quantum resonance phase (rational $\tilde{\hbar}/(4\pi)$)[1] and the localized phase (irrational $\tilde{\hbar}/(4\pi)$)[2].

[1] P. Fang, C. S. Tian and J. Wang. Symmetry and dynamics universality of supermetal in quantum chaos. Phys. Rev. B 92, 235437 (2015).
[2] C. Hainaut#, P. Fang#, A. Rançon, J. F. Clément, P. Szriftgiser, J. C. Garreau, C. S. Tian*, R. Chicireanu*, Experimental Observation of a Time-Driven Phase Transition in Quantum Chaos, PHYSICAL REVIEW LETTERS, 121, 134101 (2018).

Global bifurcation diagrams of a prescribed curvature problem arising in a generalized MEMS model

Kuo-Chih Hung

Abstract

We study global bifurcation diagrams and exact multiplicity of positive solutions for the one-dimensional prescribed mean curvature problem arising in MEMS

$$\begin{cases} -\left(\dfrac{u'(x)}{\sqrt{1+(u'(x))^2}}\right)' = \dfrac{\lambda}{(1-u)^p}, \quad u<1, \quad -L<x<L, \\ u(-L)=u(L)=0, \end{cases} \tag{1}$$

where $\lambda>0$ is a bifurcation parameter, and $p, L>0$ are two evolution parameters.

Notice (1) can be written in the equivalent dynamical system

$$\begin{cases} \dot{u}=v, \\ \dot{v}=-\lambda\dfrac{(1+v^2)^{3/2}}{(1-u)^p}, \quad u(-L)=u(L)=0. \end{cases} \tag{1*}$$

The problem is a derived variant of a *canonical* model used in the modeling of electrostatic MEMS device obeying the electrostatic Coulomb law with the Coulomb force satisfying the *inverse p-th power law* with respect to the distance of the two charged objects, which is a function of the deformation variable.

When a voltage λ is applied, the membrane deflects towards the ceiling plate and a snap-through may occur when it exceeds a certain critical value λ^*, referred to as the "pull-in voltage". This creates a so-called "pull-in instability" which greatly affects the design of many devices. Also, in the actual design of a MEMS device, typically, one of the primary device design goals is to achieve the maximum possible stable steady-state deflection (that is, $\|u_{\lambda^*}\|_\infty$ (<1), referred to as the "pull-in distance", with a relatively small applied voltage.

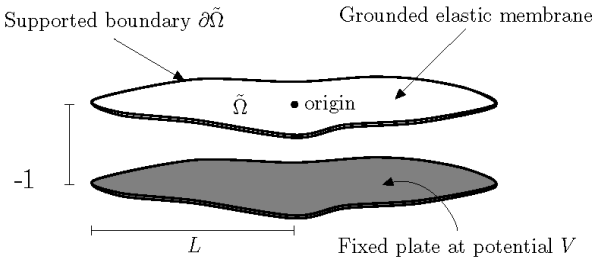

- For $p \geq 1$, the bifurcation diagram (1) undergoes *two* bifurcations. The first is a standard *fold* (or called *saddle-node*) bifurcation, which happens for all positive L at some positive λ^*. The second is a *splitting* bifurcation.

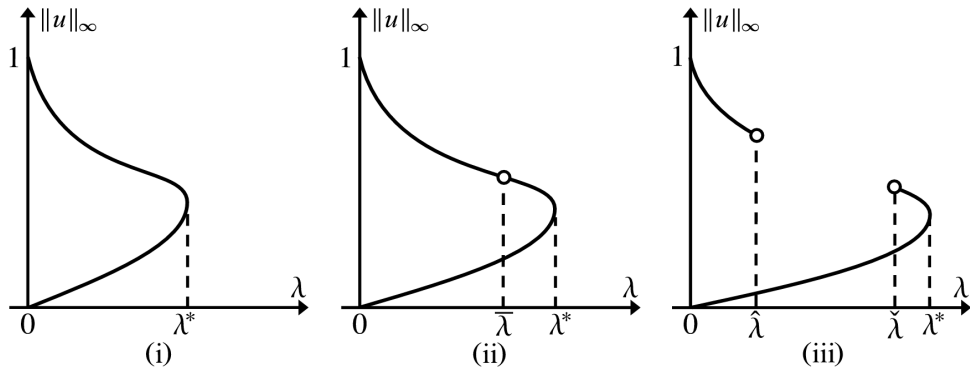

Global bifurcation diagrams $C_{p,L}$ with $p \geq 1$.
(i) $L > L^*$. (ii) $L = L^*$. (iii) $0 < L < L^*$.

- For $0 < p < 1$, the bifurcation diagram (1) undergoes *three* bifurcations. The first is a standard *fold* bifurcation. The second is a *splitting* bifurcation. The third is a *segment-shrinking* bifurcation.

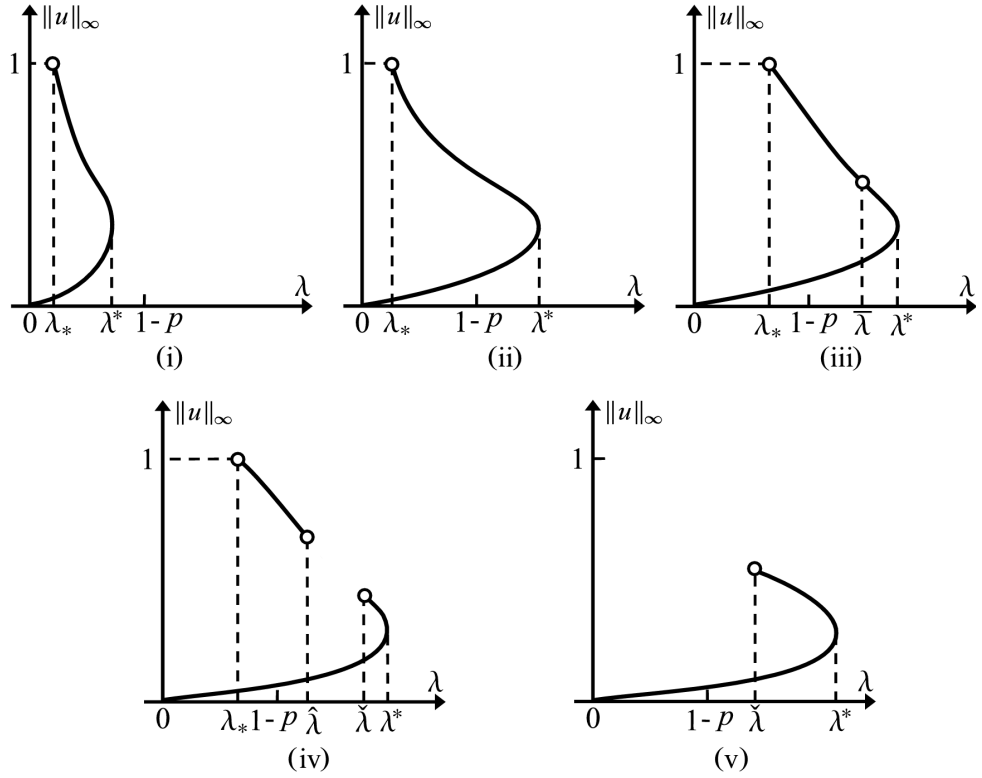

Global bifurcation diagrams $C_{p,L}$ with $0 < p < 1$.
(i)–(ii) $L > L^*$. (iii) $L = L^*$. (iv) $L_* < L < L^*$. (v) $0 < L \leq L_*$.

Evaluating the Effectiveness of Precursor Data on Earthquake Forecasting Depending on Earthquake Depth

Matheus Junqueira[a], Masanori Shiro, Yuji Yagi, Yoshito Hirata
[a] Graduate School of Science and Technology – University of Tsukuba

- Effective ways to forecast earthquakes are yet to be designed
- The literature gives evidence that external factors can change the patterns of earthquake occurrence
  - Solar magnetic field
  - Lunar tides
  - Atmospheric temperatures
- They cannot be expected that they will affect earthquakes equally regardless of depth
- Investigating how forecasting accuracy varies with the earthquake depths can give important insights on which precursors are most relevant
- Here we perform such analysis for surface temperatures and sunspot data

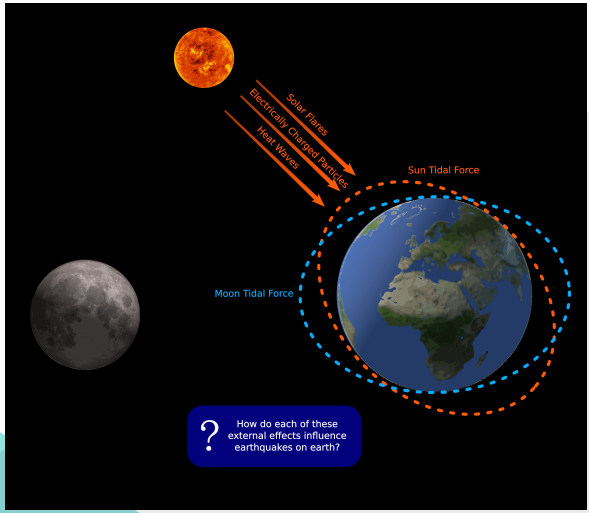

A Glimpse of the Results

all depths

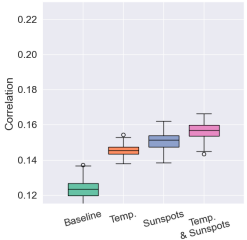

depth < 50 km

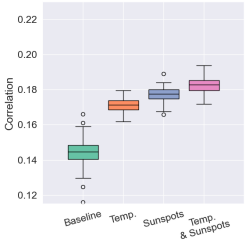

depth < 30 km

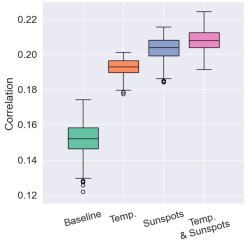

- We try to predict earthquakes in the Balkans using temperature data and/or sunspot numbers

- the correlation increases sharply as we decrease the threshold for the earthquake depths
- For earthquakes shallower than 30 km, we observe a correlation of approximately 0.21 when using both kinds of data
- An increase of $\sim 35\%$ from the baseline.
- In the "all depths" model, not only the correlations were lower, but the increase was only of $\sim 26\%$

- The results give pieces of evidence that support that depth is a very significant variable in precursor analysis
- This can also be used to reason about the mechanism by which the Sun affects earthquakes
- The evidence strongly suggests that the Sun affects earthquakes by means of the heat that it is constantly transferring to our atmosphere

Highly efficient THz wave using chaotic supremacy

Fumiyoshi Kuwashima, Mona Jarrahi, *et al.*

- Chaotic Supremacy is a new concept to express the properties that can only be realized by chaos
- Originated from ergodicity, mixture property, and structural stability of chaos.

- Autonomous system
- High-efficiency（improve energy conservation）
- Structural stability

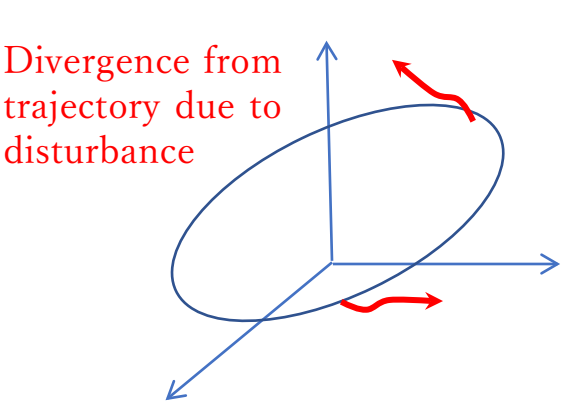

Limit cycle

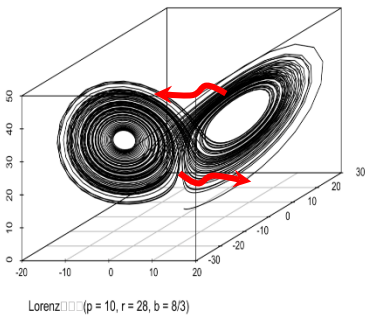

Chaos attractor
Extend to all the phasespace

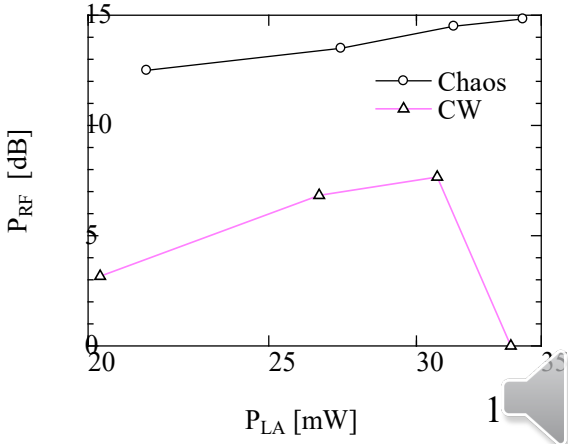

High stability and efficency

Stable optical beats near the laser threshold using laser chaos

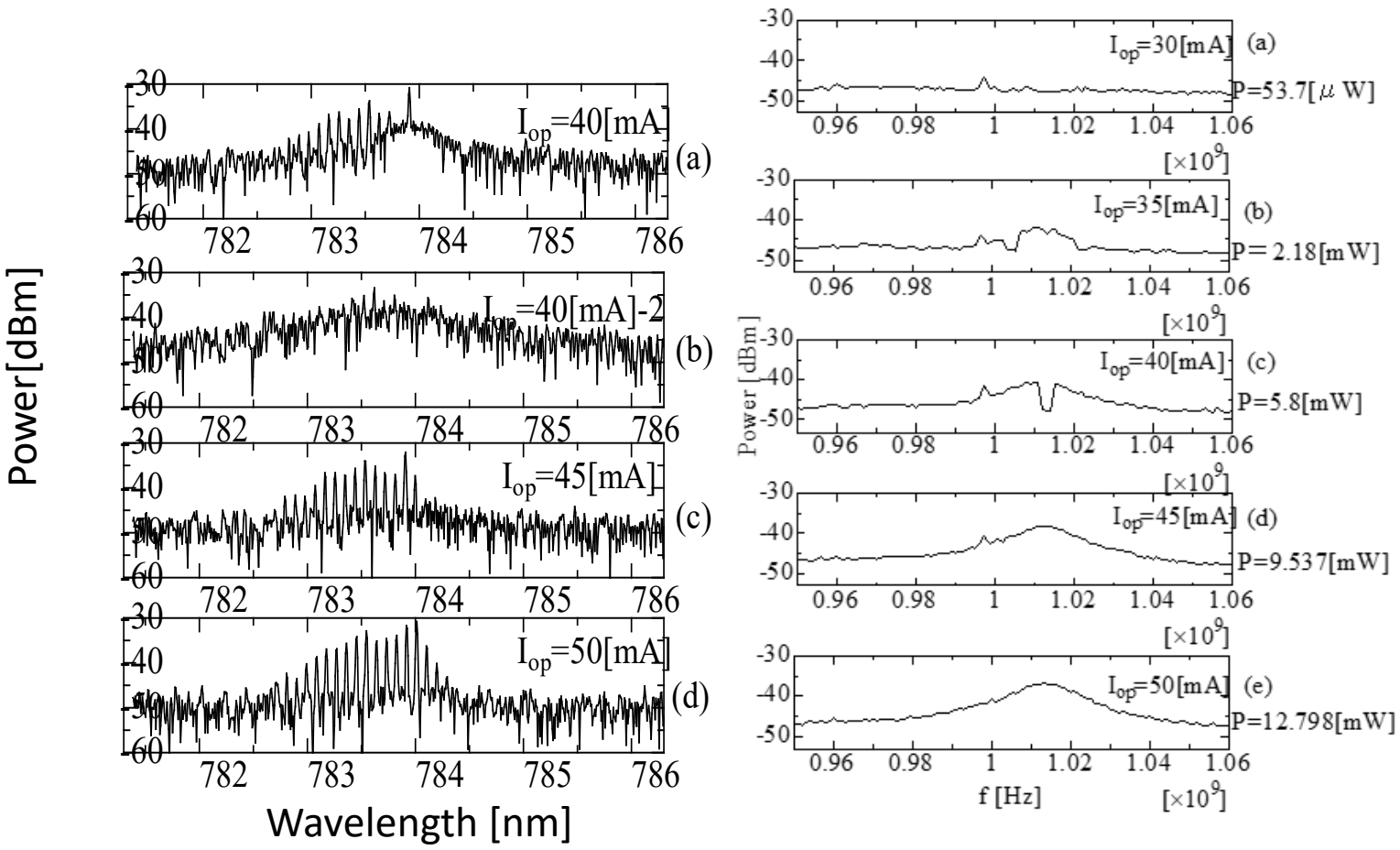

Emergent Dynamic Patterns in Chemokinetic Active Matter with Fuel Consumption

Euijoon Kwon, Yongjae Oh, and Yongjoo Baek

Department of Physics and Astronomy, Seoul National University, Seoul, Republic of Korea

Noneq. Stat. Phys. Lab @ SNU

Introduction

- Active matter shows collective behavior which comes from the nonequilibrium nature of the system.

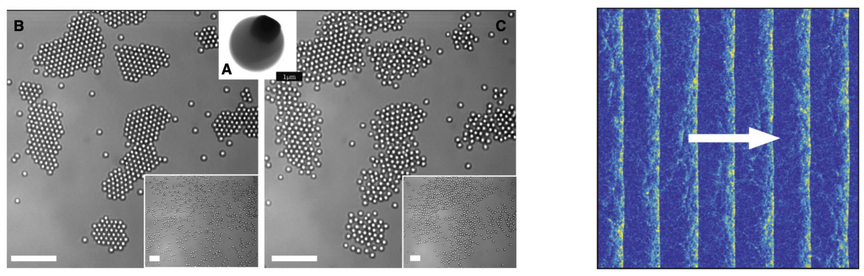

- Recently, the role of chemical signaling on active matter have been studied extensively, where many of them focuses on chemotaxis.
- On the other hand, the effect of fuel depletion due to local consumption is neglected in previous active matter models.
- Motivated by this, we investigate chemokinetic active particle (CAP) with fuel consumption, and study the interplay between clustering of CAPs and chemical diffusion.

Two mechanisms of fuel consumption

Basal Metabolic Regime (BMR)

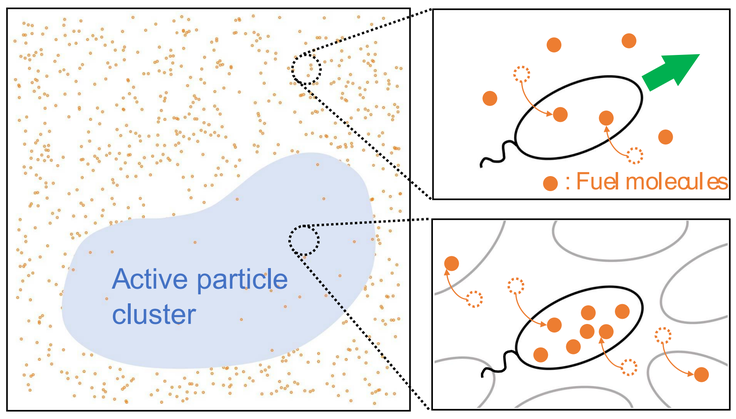

- The fuel consumption rate is proportional to the density of the active particles
- Inside the dense cluster, fuel is depleted by large consumption of CAPs, which results in the slowdown of CAPs

→ Phase separation is enhanced (positive feedback)

Active Metabolic Regime (AMR)

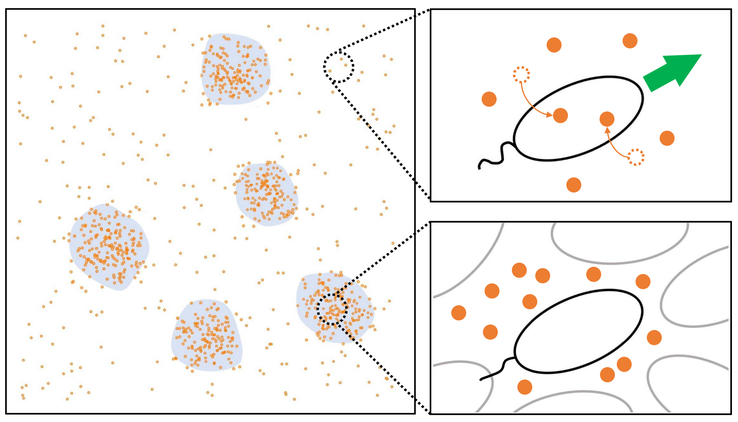

- the fuel consumption rate is proportional to the actual distances traveled by CAPs.
- Inside the dense cluster, fuel is piled up due to stuck motion of CAPs, which helps CAPs to escape the cluster

→ Phase separation is suppressed (negative feedback)

The model: particle-based description

- Chemokinetic active particles

$$\dot{\mathbf{r}}_k = \mu v[\rho_{\text{local}}, n]\,\hat{\mathbf{e}}_k + \sqrt{2\mu T}\,\xi_k, \qquad v[\rho_{\text{local}}, n] = \alpha n - \zeta \rho_{\text{local}}$$

- Fuel

$$\dot{n}(\mathbf{r},t) = \underbrace{D_c\,\nabla^2 n}_{\text{diffusion}} + \underbrace{I}_{\text{global injection}} - \lambda\, f(n,\{\mathbf{r}_k,\dot{\mathbf{r}}_k\}) \quad \text{local consumption}$$

$$f(n,\{\mathbf{r}_k,\dot{\mathbf{r}}_k\}) = \begin{cases} \int d^2\mathbf{r}'\, n(\mathbf{r})\,\delta(\mathbf{r}-\mathbf{r}')\sum_{k'=1}^{N}\delta(\mathbf{r}'-\mathbf{r}_{k'}), & \text{BMR} \\ \int d^2\mathbf{r}'\, n(\mathbf{r})\,\delta(\mathbf{r}-\mathbf{r}')\sum_{k'=1}^{N}\dot{\mathbf{r}}_{k'}\cdot\hat{e}_{k'}\delta(\mathbf{r}'-\mathbf{r}_{k'}), & \text{AMR} \end{cases}$$

Coarse-grained continuum description

- Coarse-grained hydrodynamic equation

$$\dot{\rho}(\boldsymbol{r},t) = \boldsymbol{\nabla}\cdot\left[D\,\boldsymbol{\nabla}\rho + \frac{v(\rho,n)}{2D_{\mathrm{r}}}\boldsymbol{\nabla}[v(\rho,n)\rho] - \kappa\boldsymbol{\nabla}(\boldsymbol{\nabla}^2\rho)\right]$$

$$\dot{n}(\boldsymbol{r},t) = D_c\boldsymbol{\nabla}^2 n + I - \begin{cases}\lambda\rho n, & \text{BMR}\\ \lambda\rho v(\rho,n)n, & \text{AMR}\end{cases}$$

Video

Linear stability analysis & numerical simulation

- BMR (basal metabolic regime)

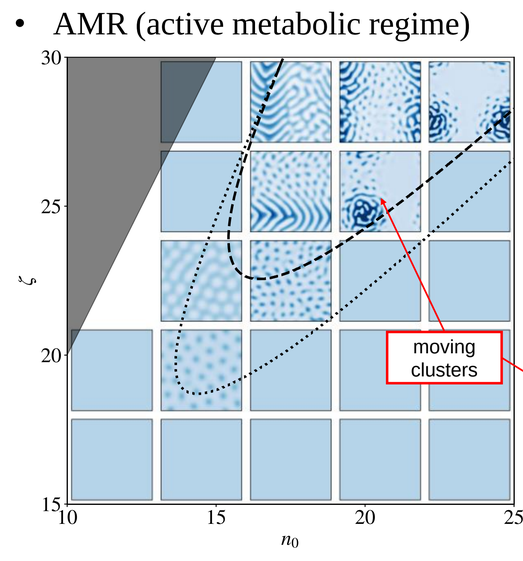

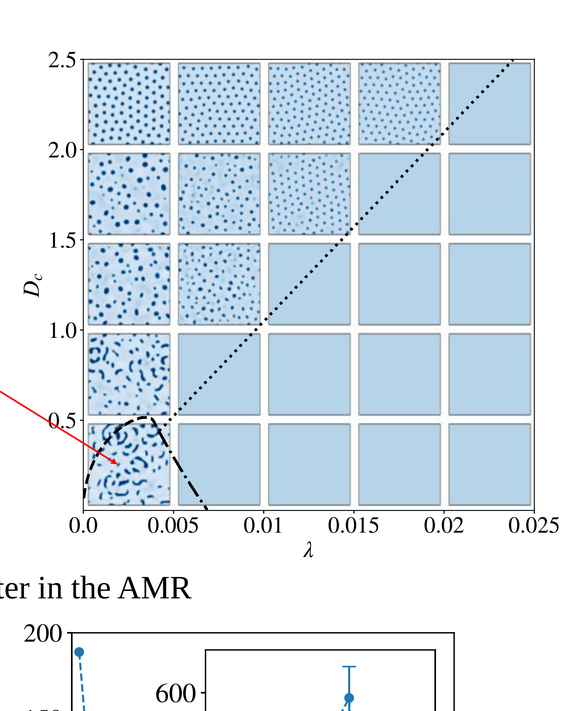

- AMR (active metabolic regime)

- Microphase separation & moving cluster in the AMR

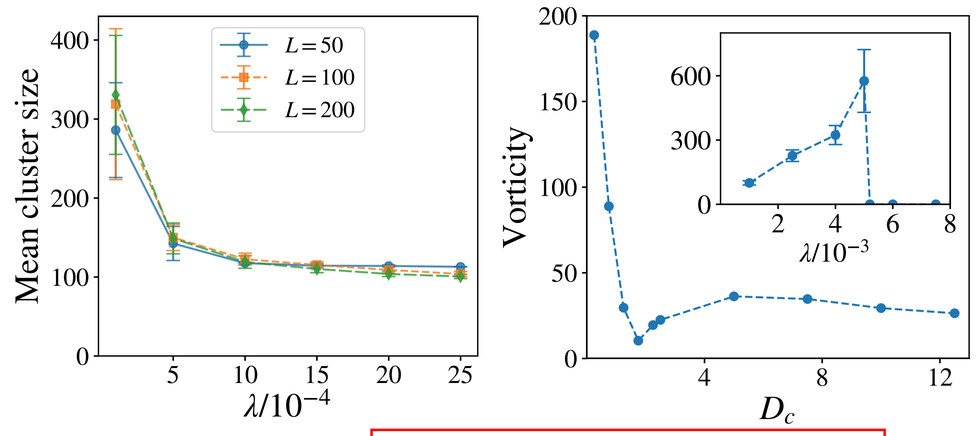

Vorticity= $\frac{1}{L^2}\int d^2\boldsymbol{r}\,\left|\boldsymbol{\nabla}\times\frac{\boldsymbol{j}}{\rho}(\boldsymbol{r})\right|^2$ (j: current of the system)

Particle-based simulation

- WCA potential

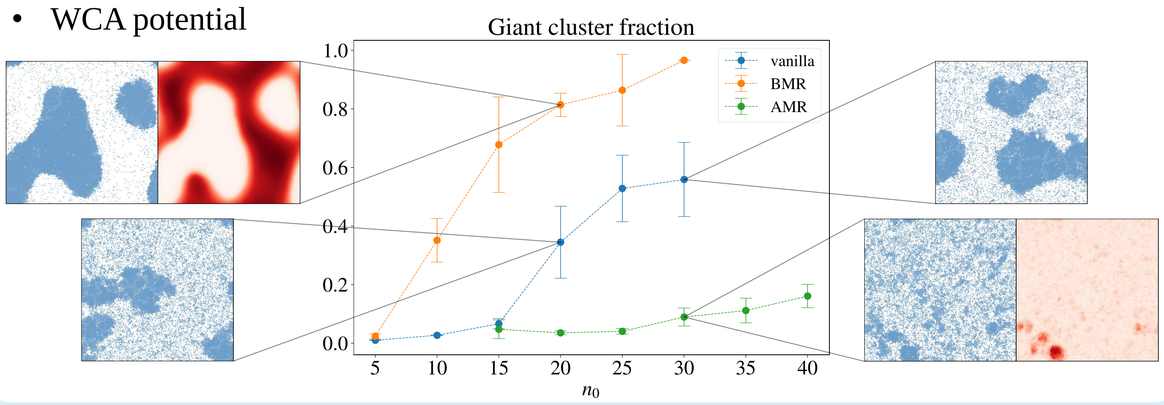

Conclusion

- We investigate how the changes in the self-propulsion strength via fuel depletion affect the MIPS phenomenology of active particle.
- In the BMR, the phase separation is always enhanced.
- In the AMR, the phase separation is suppressed with microphase separation and emergent oscillatory patterns.
- Our possible future works include investigating the role of fuel consumption in other active matter system (polar, chiral, etc.) and experimental confirmation of our results.

Inference of coupling network of oscillatory systems using the circle map

Akari Matsuki (Hokkaido University, Japan)

R.Kobayashi H.Kori

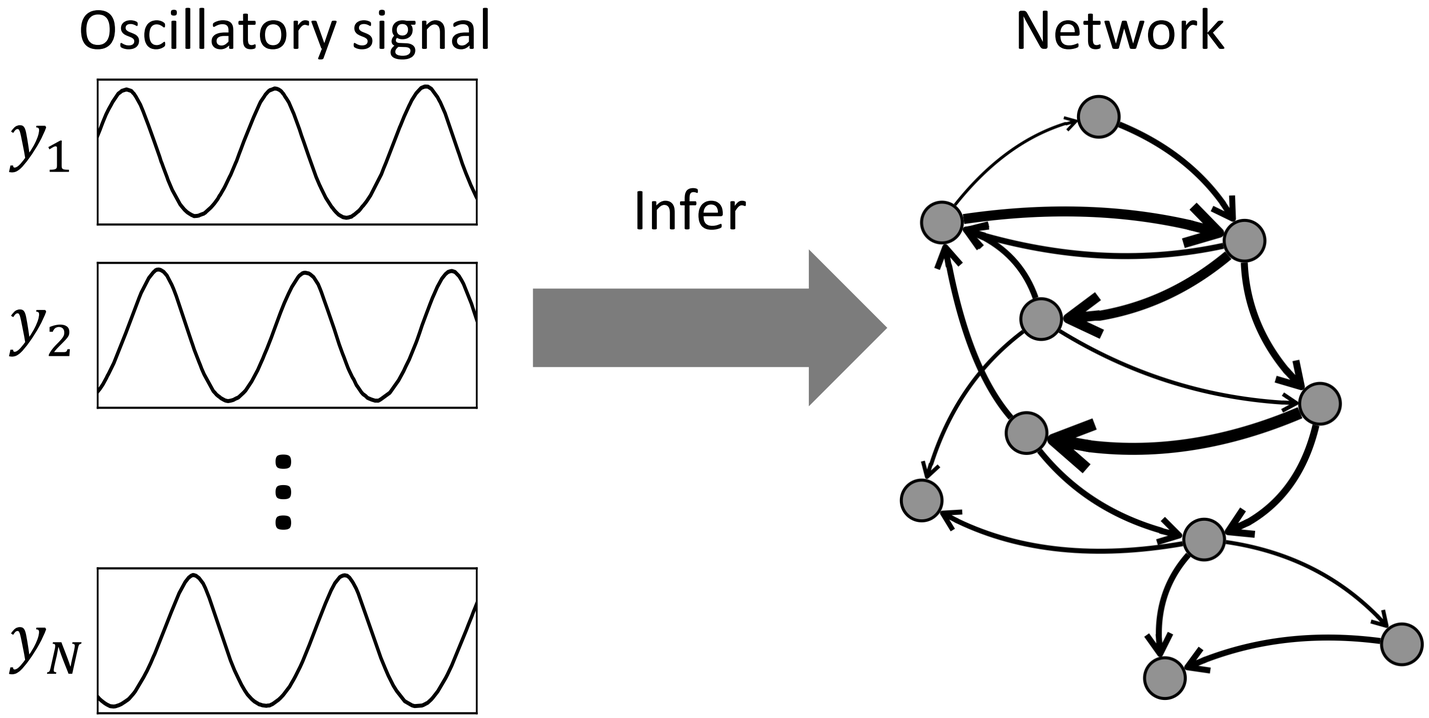

We propose circle-map-based inference

We fit data to a phase model. Which model to use?

Clock cell network

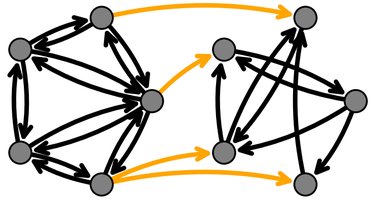

Naive: Kuramoto model

$$\dot{\phi}_i = \omega_i + \sum_{j=1}^{N} c_{ij} \sin(\phi_j - \phi_i + \alpha) + \xi_i(t)$$

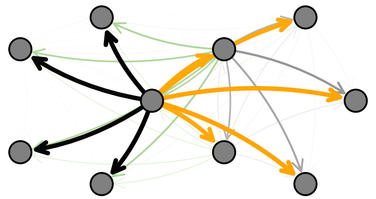

Propose: Circle map

$$\frac{\phi_i(t+T) - \phi_i(t)}{T} = \omega_i + \sum_{j=1}^{N} c_{ij} \sin(\phi_j - \phi_i + \alpha) + \xi_i(t)$$

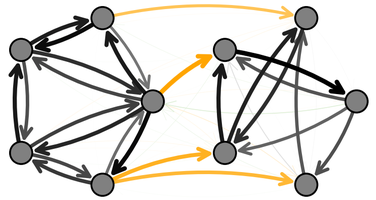

Accurate!

Signatures of Quantum Chaos and fermionization in the incoherent transport of bosonic carriers in the Bose-Hubbard chain

P. S. Muraev ,[1,2] D. N. Maksimov, [1,3] and A. R. Kolovsky [2,3]
1 IRC SQC, Siberian Federal University, 660041 Krasnoyarsk, Russia
2 School of Engineering Physics and Radio Electronics, Siberian Federal University, 660041 Krasnoyarsk, Russia
3 Kirensky Institute of Physics, Federal Research Center KSC SB RAS, 660036 Krasnoyarsk, Russia

Introduction

One of the central questions to be addressed with the open BH chain, both theoretically and experimentally, is the stationary current of Bose particles across the chain and its dependence on the strength of interparticle interactions. To approach the outlined problem, we introduce a specific boundary driven BH model which conserves the number of particles in the system. Although the introduced model cannot be directly related to ongoing laboratory experiments, it admits a comparative theoretical analysis with the closed BH system.

The Model

We consider the BH chain of the length L with incoherent coupling between the first and the Lth sites. The coupling is described by the following Lindblad operators

$$\hat{\mathcal{L}}_1(\hat{\mathcal{R}}) = \hat{V}^\dagger\hat{V}\hat{\mathcal{R}} - 2\hat{V}\hat{\mathcal{R}}\hat{V}^\dagger + \hat{\mathcal{R}}\hat{V}^\dagger\hat{V},$$

$$\hat{\mathcal{L}}_2(\hat{\mathcal{R}}) = \hat{V}\hat{V}^\dagger\hat{\mathcal{R}} - 2\hat{V}^\dagger\hat{\mathcal{R}}\hat{V} + \hat{\mathcal{R}}\hat{V}\hat{V}^\dagger,$$

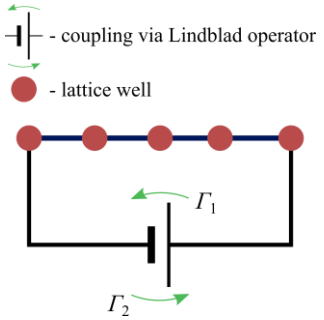

where $\hat{V} = \hat{a}_1^\dagger\hat{a}_L$. Thus, the master equation for the carrier density matrix $\hat{\mathcal{R}}$ reads

$$\frac{\mathrm{d}\hat{\mathcal{R}}}{\mathrm{d}t} = -i[\hat{\mathcal{H}}, \hat{\mathcal{R}}] - \Gamma_1\hat{\mathcal{L}}_1 - \Gamma_2\hat{\mathcal{L}}_2,$$

where

$$\hat{\mathcal{H}} = -\frac{J}{2}\sum_{l=1}^{L-1}(\hat{a}_{l+1}^\dagger\hat{a}_l + \mathrm{H.c.}) + \frac{U}{2}\sum_{l=1}^{L}\hat{n}_l(\hat{n}_l - 1)$$

is the Bose-Hubbard Hamiltonian.

Results

We demonstrate that the system described above exhibits different transport regimes. These regimes are determined by the ratio between the tunneling and interaction constants in the Bose-Hubbard Hamiltonian. Additionally, we will show that the nonequilibrium many-body density matrix of the bosonic carriers in the chain exhibits a transition from a regular spectrum to an irregular one.

Delay induced transient dynamics with resonance and resurgence

Kenta Ohira, Graduate School of Informatics, Nagoya University

We propose simple delay differential equation whose solutions can be constructed.

$$\frac{dX(t)}{dt} + atX(t) = bX(t-\tau),$$

Transient oscillation appears and disappears with the increasing value of the delay showing a frequency resonance.

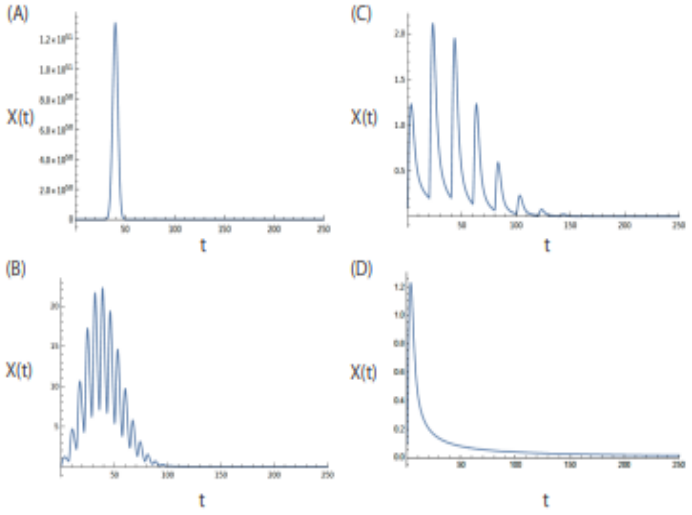

Power Spectrum exactly obtained:

$$S(\omega) = |\hat{X}(\omega)|^2 = \hat{X}(\omega)\hat{X}^*(\omega) = \mathcal{C}^2 \mathrm{Exp}\left[-\frac{1}{a}\omega^2 + \frac{2b}{\tau a}\cos\omega\tau\right].$$

a = 0.15, b = 6.0 τ : (A) 0, (B) 7, (C)20, (D)∞

The Lambert W function

$W : C \to C$ satisfying

$$W(z)e^{W(z)} = z \tag{10}$$

The branches of the W function are expressed as $W_k, k = 0, \pm 1, \pm 2, \ldots, \pm\infty$.

Exact Solution Construction with the W function

$$\frac{dX(t)}{dt} + atX(t) = be^{-a\tau t}X(t-\tau).$$

$$X(t) \approx X_0 e^{-\frac{1}{2}at^2} Re[e^{\frac{1}{\tau}W_0(\ddot{b}\tau)t}] = X_0 e^{-\frac{1}{2}at^2} e^{\frac{1}{\tau}Re[W_0(\ddot{b}\tau)]t} \cos(\frac{1}{\tau}Im[W_0(\hat{b}\tau)]t)$$

$$\hat{b} = \hat{b}(\tau) = be^{-\frac{1}{2}a\tau^2}$$

Using such exact solution, various peculiar transient dynamics induced by delay can be analyzed

P20. Measurement-only dynamical phase transition of topological and boundary order in toric code and gauge-Higgs models

Institute for Solid State Physics, The University of Tokyo, Takahiro Orito

Projective measurement

Entangled state (Bell state)

$$|\Psi\rangle = \frac{1}{\sqrt{2}}(|\uparrow_1\uparrow_2\rangle + |\downarrow_1\downarrow_2\rangle)$$

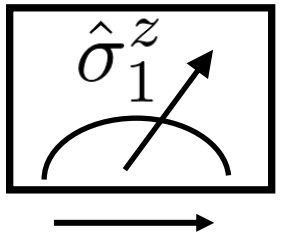

Product state

$$|\Psi\rangle = |\uparrow_1\uparrow_2\rangle \text{ or } |\Psi\rangle = |\downarrow_1\downarrow_2\rangle$$

Does any measurement reduce entanglement?

Product state

$$|\Psi\rangle = |\uparrow_1\uparrow_2\rangle$$

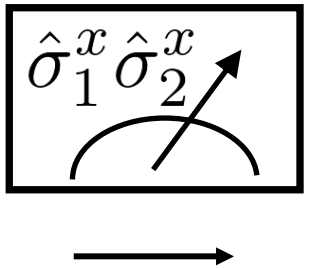

Entangled state (Bell state)

$$|\Psi\rangle = \frac{1}{\sqrt{2}}(|\uparrow_1\uparrow_2\rangle + |\downarrow_1\downarrow_2\rangle)$$

or

$$|\Psi\rangle = \frac{1}{\sqrt{2}}(|\uparrow_1\uparrow_2\rangle - |\downarrow_1\downarrow_2\rangle)$$

Measurement can induce entanglement

P20. Measurement-only dynamical phase transition of topological and boundary order in toric code and gauge-Higgs models

Institute for Solid State Physics, The University of Tokyo, Takahiro Orito

Quantum circuit

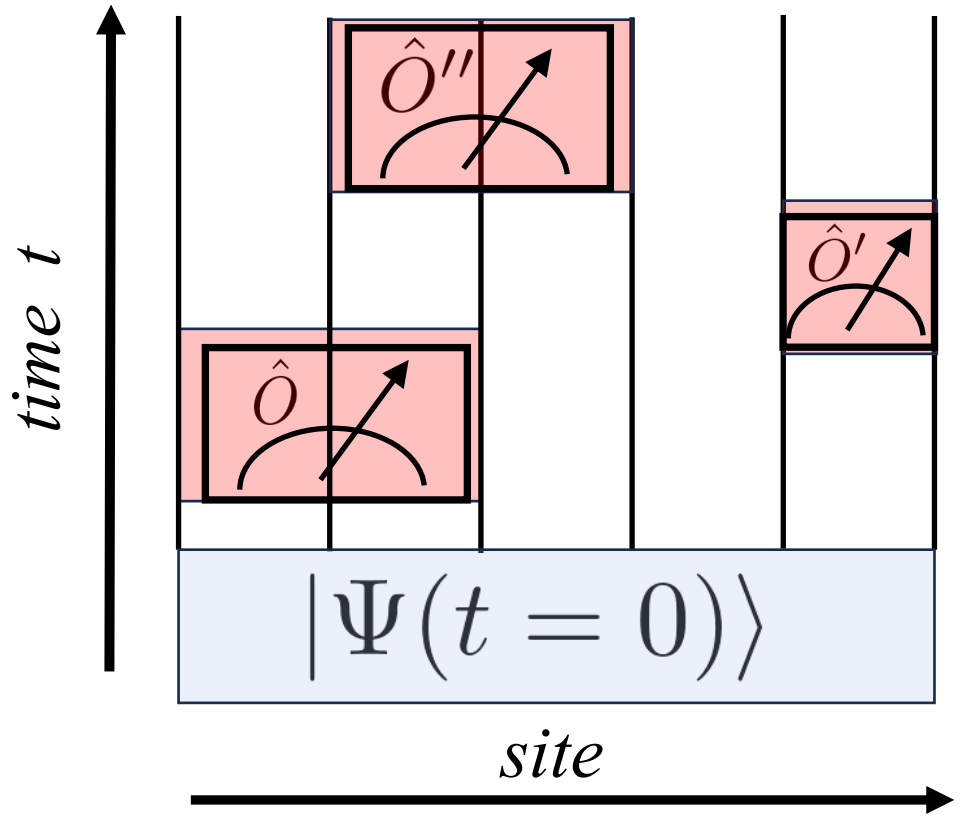

Toric code like circuit

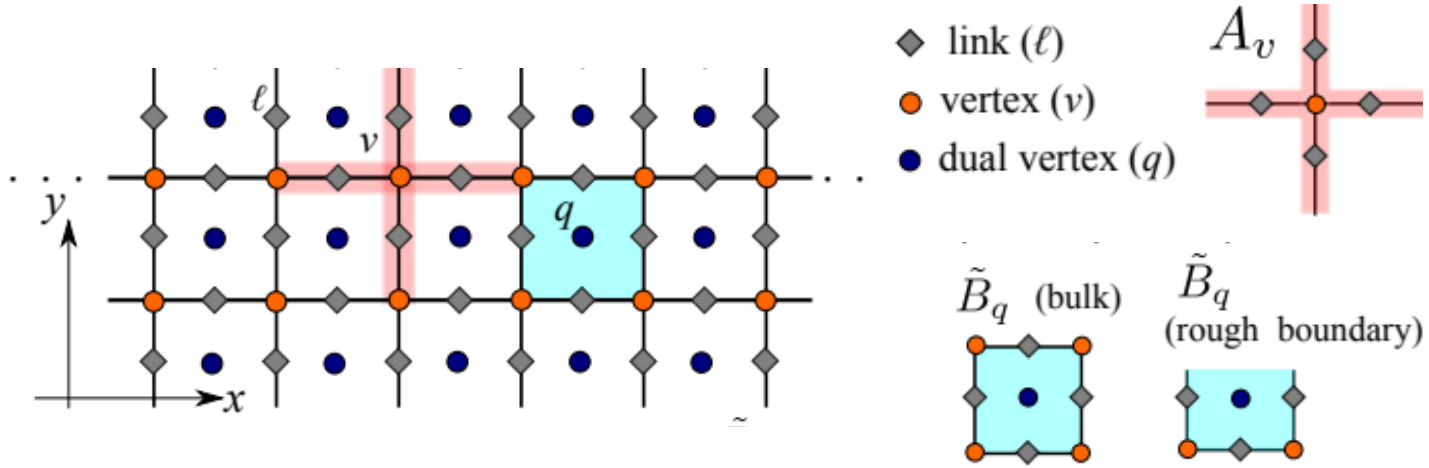

Target

Non-equilibrium behavior of toric code like circuit and topological and boundary order

Measurement induces "dynamics"

Please Visit!!

Extreme Events Scaling in Finite-Size Abelian Sandpile Model

Abelian BTW Sandpile Model

- The emergent scale-invariant feature remains one of the most remarkable observation occurring in system.
- Such features can arise near the critical point of a continuous transition between order and disorder phases.
- The concept of Self-organized criticality introduced by Bak et al. (1987), explains the underlying origin of scaling in natural systems, which remain far away from equilibrium.
- Observable x can describe the events like size (total toppled sites) s and area (spatial extent of size) a, duration T.

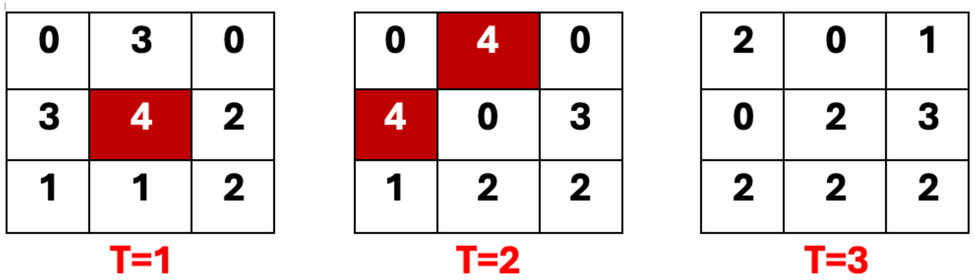

- The probability distribution of the event x obeys a decaying power-law behavior

$$P(x, x_c) = \begin{cases} A x_c^{-\theta} x^{-\tau_x}, & \text{for } x \ll x_c \\ \text{rapid change}, & \text{for } x \approx x_c \end{cases}$$

Generalized Extreme Value Distribution

$$\mathcal{F}(x; \mu, \beta, \xi) = \exp\left\{ -\left[1 + \xi\left(\frac{x - x_c}{\beta}\right)\right]^{-1/\xi} \right\}$$

where x_c, β and ξ are location (or mode), scale, and shape parameters, respectively, having bounds x_c, $\xi \in \mathbb{R}$ and $\beta \in \mathbb{R} \mid \beta > 0$. Depending upon the valued of shape parameter can be categorised into three universality classes

i. $\xi > 0$ implies Fr\'echet class where the parent distribution decaying as a power law.

ii. $\xi < 0$, describes Fisher - Tippette - Gumbel (FTG) class for which the parent distribution decays faster than power law.

iii. $\xi = 0$ represents Gumbel class

Methodology

1. Peak over threshold
2. Block Maxima

Objectives:

➡ Extreme activity distribution may also be an explicit function of the system size.

➡ The probability, along with the parameters, may vary with the system size and belong to the same class of extreme value distributions.

➡ We demonstrate a simple scaling analysis that can capture this characteristic.

Abdul Quadir* and Haider H Jafri, Department of Physics, Aligarh Muslim University, Aligarh INDIA

Results and Discussions

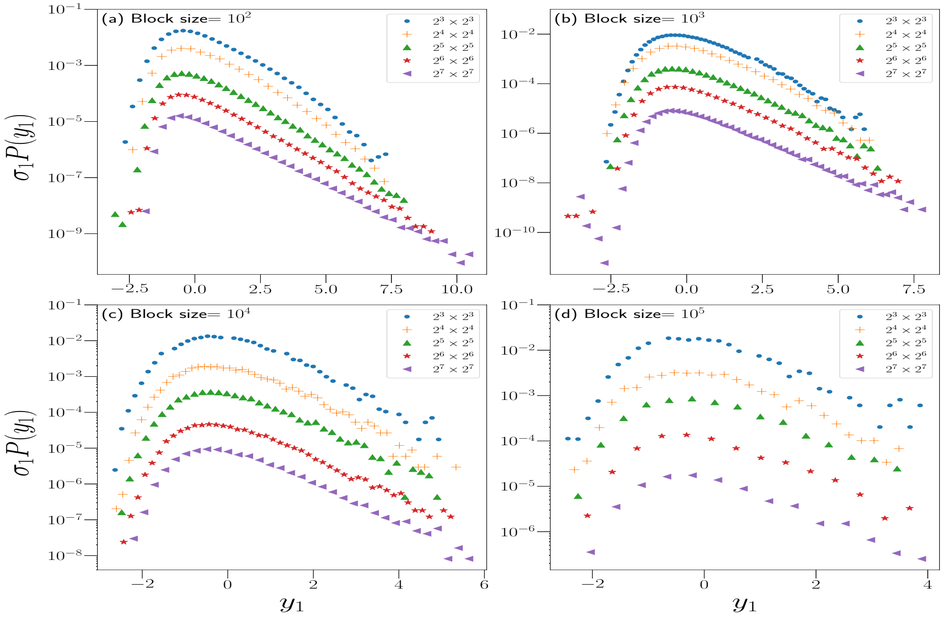

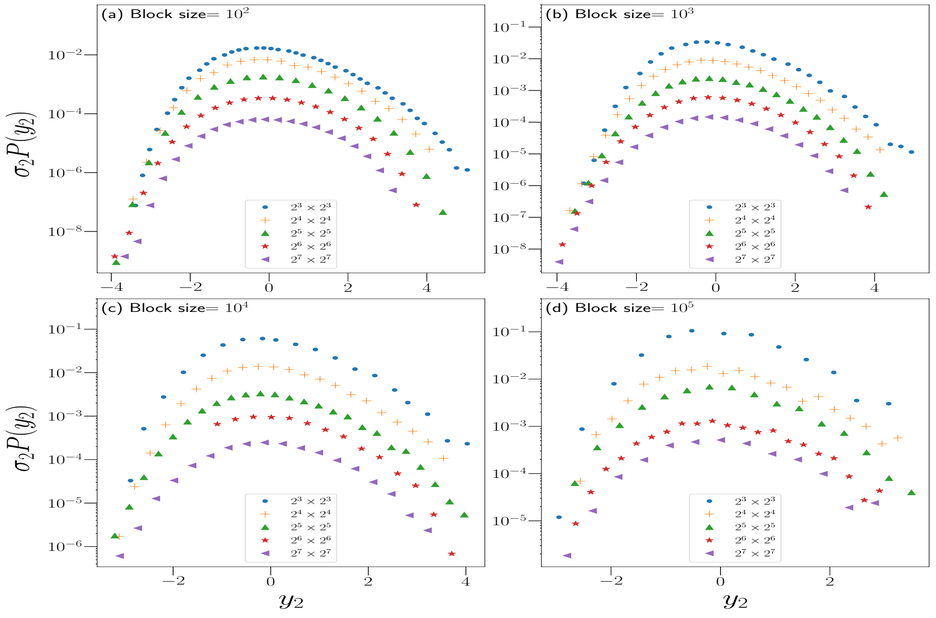

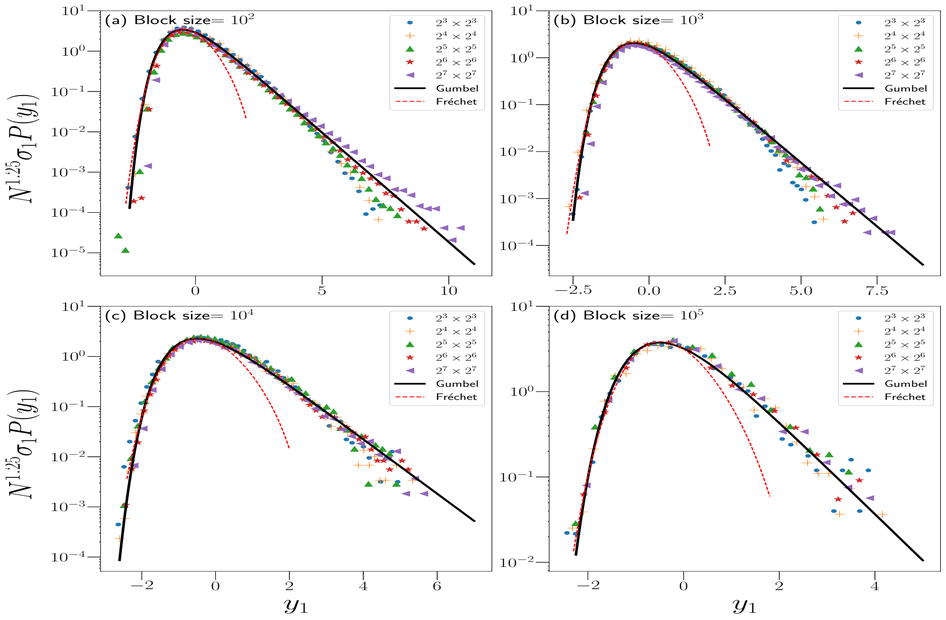

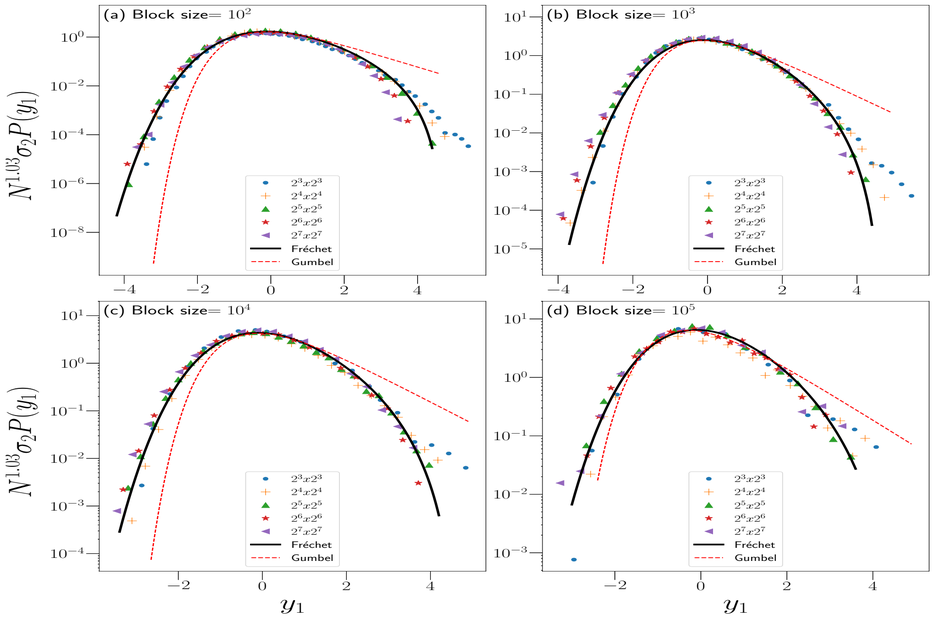

Extreme value distributions and data collapse for maxima of avalanche sizes with different block size

Extreme value distributions and data collapse for maxima of avalanche area with different block size

We found that:

$$\langle x_i \rangle = \langle x_i(N) \rangle \sim N^{\alpha}$$

Rescaling: $y_i = \dfrac{x_i - \langle x_i \rangle}{\sigma_i}$

We observe that:

$$\begin{cases} P(y_1 = y_c) \sim N^{-\gamma_1}, & \gamma_1 = 1.25 \\ P(y_1 = y_c) \sim N^{-\gamma_2}, & \gamma_1 = 1.05 \end{cases}$$

Scaling Function:

$$\psi(x_j; N) = N^{-\gamma_j} \frac{1}{\sigma_j} \mathscr{F}\left(\frac{x_j - \langle x_j \rangle}{\sigma_j} \right)$$

Numerically we found that:

- ✓ Avalanche size maxima lies into Gumbel family of GEVD with $\xi = 0.0$
- ✓ Avalanche size maxima lies into Frechet family of GEVD with $\xi = 0.19$

Active Granular Nematics

Abhishek Sharma

Supervisor: Dr. Harsh Soni

Indian Institute of Technology Mandi, India-175005

Dynamics Days Asia Pacific 13 / YKIS2024

July, 2024

1. Introduction

- Active matter in nature:

Bird Flock

https://www.nature.com/collections/hvczfmjfzl

Fish School

https://researchfeatures.com/schooling-fish-pay-attention-neighbours-coordinating-their-collective-movements/

2. Active granular nematic system

- Experimental setup:

-A. K. Sood lab

- Simulation model:

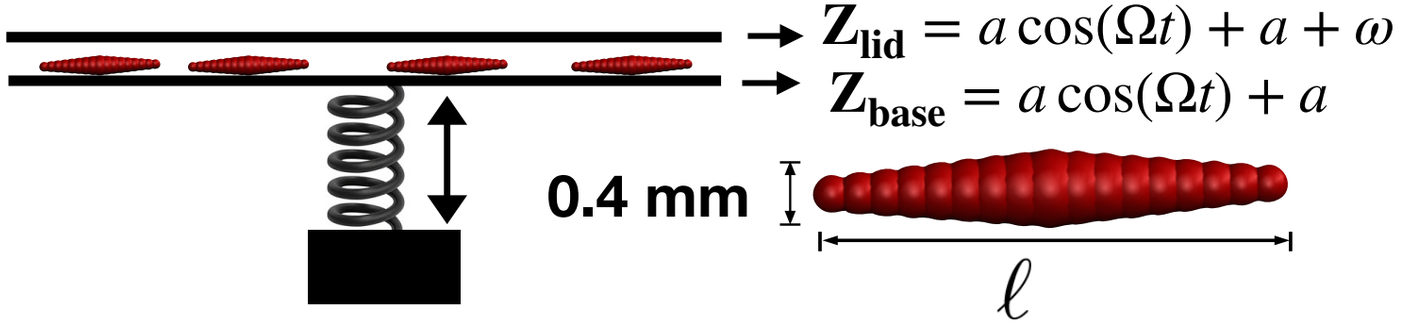

3.Main key findings

- Phase diagram in (ϕ-ℓ) plane

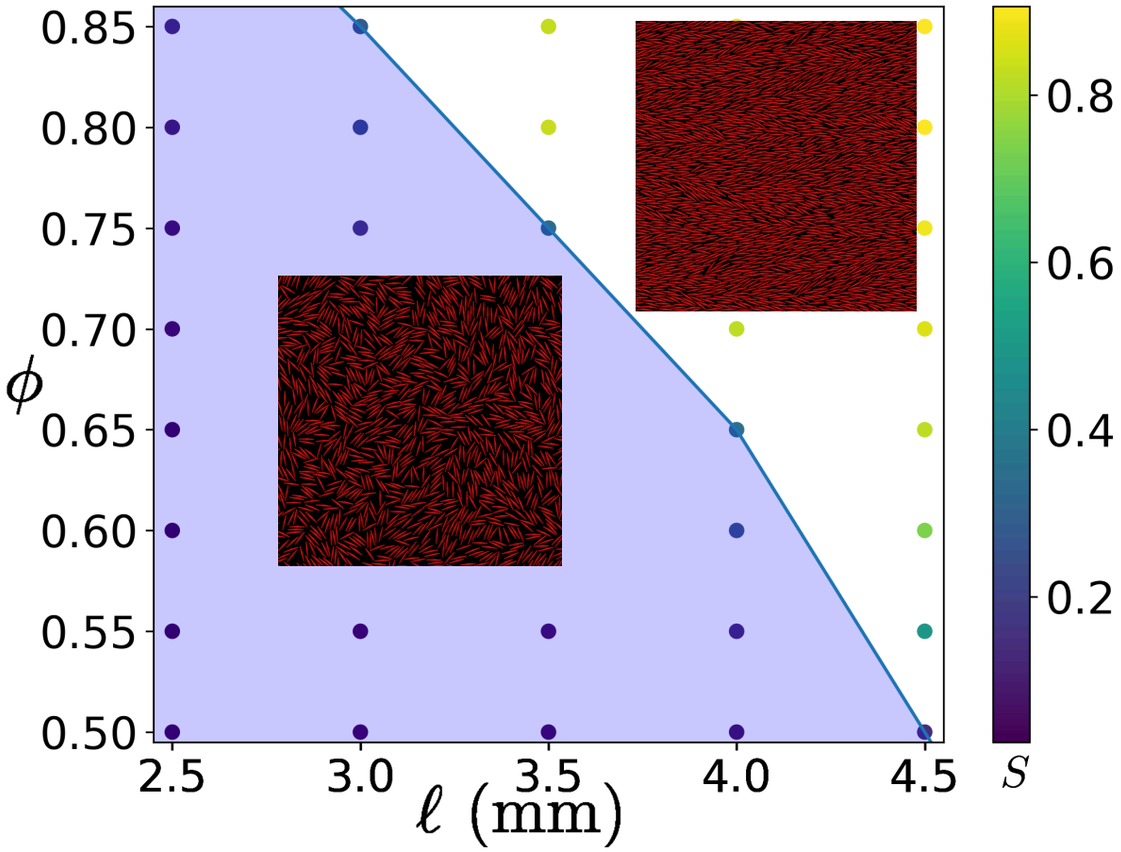

- $G_2(\mathbf{r})$

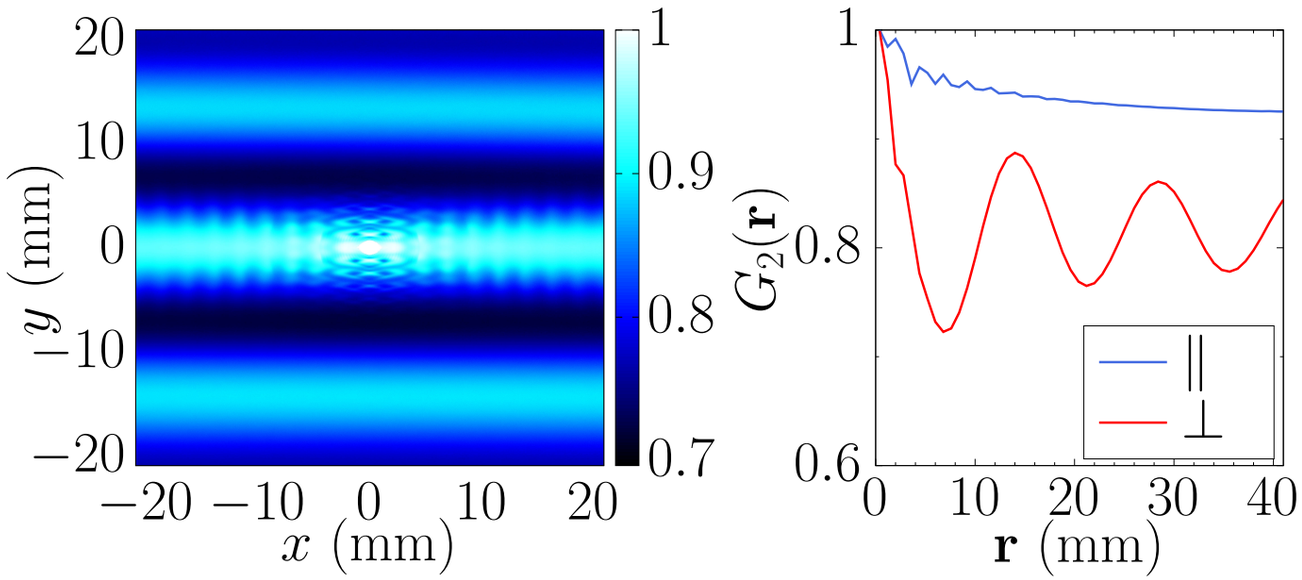

- Phase with periodic ordering and distribution function of orientation of rods $P(\theta)$

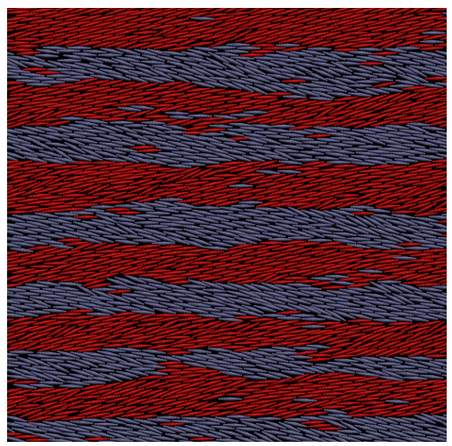

$\ell = 4.5$ mm, $\phi = 0.85$

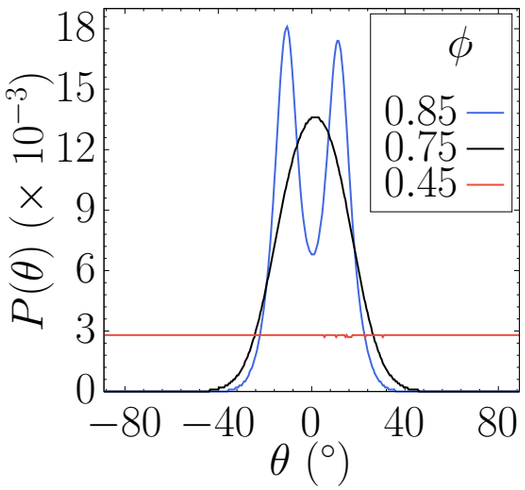

- Mean square displacement $\langle \Delta \mathbf{r}^2 \rangle$

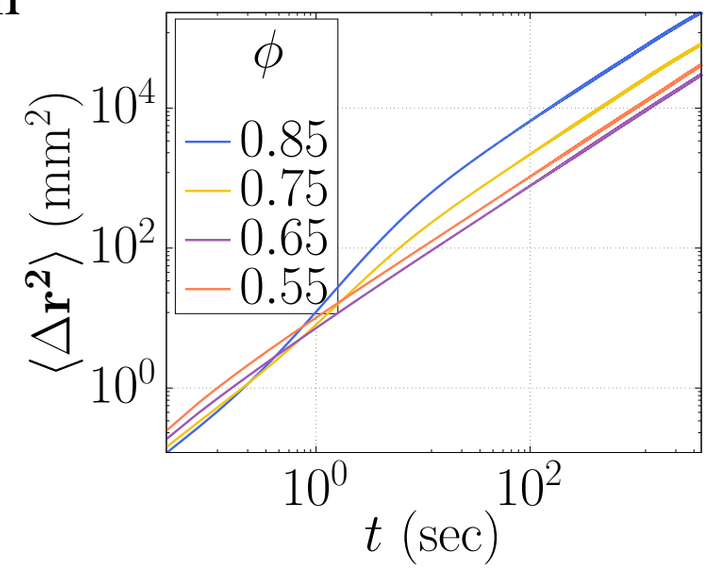

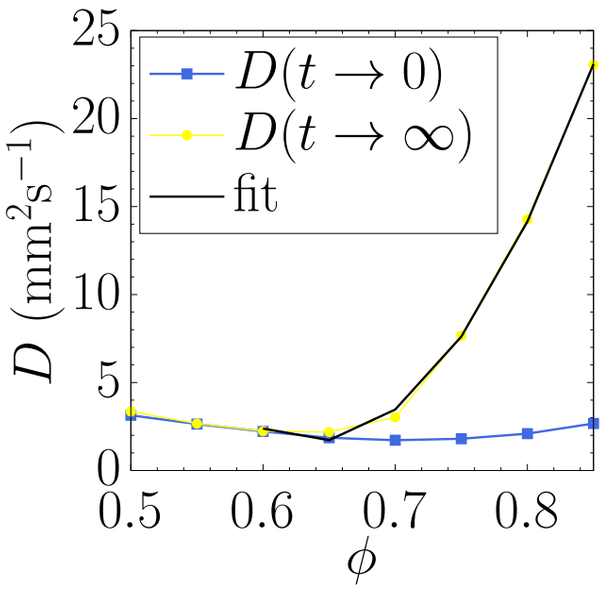

Dynamics of large oscillator populations with random interactions

Lev A. Smirnov
Department of Control Theory, Lobachevsky State University of Nizhny Novgorod, Russia

Arkady Pikovsky
Institute of Physics and Astronomy, University of Potsdam, Germany

Populations of globally coupled oscillators appear in different fields of physics, engineering, and life sciences. In many situations, there is disorder in the coupling, and the coupling terms are not identical but vary, for example, due to different coupling strengths and phase shifts. While the phenomenon of collective synchronization in oscillator populations which attracted much interest in the last decades is well-understood in a regular situation, the influence of disorder remains a subject of intensive current studies. The disordered case is relevant for many applications, especially in neuroscience, where in the description of the correlated activity of neurons, one can hardly assume the neurons themselves to be identical and the coupling between them to be uniform.

We explore large populations of rorators $\varphi_k(t)$ $(k = 1, \dots, N)$ interacting via random coupling functions:

$$\mu\ddot{\varphi}_k + \dot{\varphi}_k = \omega_k + \sigma\xi_k(t) + H\big(\{\varphi_j(t)\}\big), \tag{1}$$

where each $\varphi_k(t)$ is assumed to be a phase or an angle variable with a first-order ($\mu = 0$) or a second-order($\mu \neq 0$) in time dynamics, respectively. Here, we assume that the individual phase dynamics of an oscillator is described within the "standard" model as rotations with a natural frequency ω_k, possibly with individual Gaussian white noises $\sigma\xi_k(t)$. In Eq. (1), we separate this individual dynamics and the coupling terms $H\big(\varphi_1(t), \varphi_2(t), \dots, \varphi_N(t)\big) = H\big(\{\varphi_j(t)\}\big)$. Note that the model (1) with $\mu = 0$ corresponds to the model of coupled phase oscillators which is most popular because it can be directly derived for generic coupled oscillators from the original equations governing the oscillator dynamics, in the first order in the small parameter describing the coupling. The model (1) with $\mu \neq 0$ are discussed in the literature, for example, in the context of modeling power grads.

Next, we specify the coupling terms $H\big(\{\varphi_j(t)\}\big)$ according to the Kuramoto-Daido and the Winfree approaches. In both two cases, we assume that all the pairwise coupling terms are different, taken from some random distribution of random functions. In this assumption that all the coupling terms are generally different, the coupling function in the Kuramoto-Daido form as a function of phase differences $(\varphi_j - \varphi_k)$ reads

$$H_{KD}\big(\{\varphi_j(t)\}\big) = \frac{1}{N}\sum_{j=1}^{N} F_{jk}(\varphi_j - \varphi_k). \tag{2}$$

For the Winfree-type model, in a such case of the general randomness case, the action on the oscillator k from the oscillator j is proportional to the product $S_{jk}(\varphi_k)Q_{jk}(\varphi_j)$, where $S_{jk}(\varphi_k)$ is the j-th phase sensitivity function of the unit k, and $Q_{jk}(\varphi_j)$ describe the force with which the element j is acting on the oscillator k:

$$H_W\big(\{\varphi_j(t)\}\big) = \frac{1}{N}\sum_{j=1}^{N} S_{jk}(\varphi_k)Q_{jk}(\varphi_j). \tag{3}$$

It is well known that, in the regular setups, the Kuramoto-Daido and the Winfree coupling functions can be reformulated in terms of the Kuramoto-Daido order parameters $Z_m(t)$ which are defined as

$$Z_m(t) = \frac{1}{N}\sum_{j=1}^{N} e^{\mathrm{i}m\varphi_j(t)} = \left\langle e^{\mathrm{i}m\varphi_j(t)} \right\rangle. \tag{4}$$

One can obtain these representations representing the 2π-periodic coupling functions as Fourier series. We use these expressions as "templates" for identifying the effective coupling functions in the case of random interactions.

Thus, we represent the functions $F_{jk}(x)$, $S_{jk}(x)$ and $Q_{jk}(x)$ describing random pairwise interactions in the Kuramoto-Daido and the Winfree models via random complex Fourier coefficients $f_{m,jk}$, $s_{m,jk}$ and $q_{m,jk}$, respectively:

$$F_{jk}(x) = \sum_m f_{m,jk} e^{\mathrm{i}mx}\,, \quad S_{jk}(x) = \sum_m s_{m,jk} e^{\mathrm{i}mx}\,, \quad Q_{jk}(x) = \sum_m q_{m,jk}\, e^{\mathrm{i}mx}\,, \tag{5}$$

$$f_{m,jk} = \frac{1}{2\pi}\int_0^{2\pi} dx\, F_{jk}(x) e^{-\mathrm{i}mx}\,, \quad s_{m,jk} = \frac{1}{2\pi}\int_0^{2\pi} dx\, S_{jk}(x) e^{-\mathrm{i}mx}\,, \quad q_{m,jk} = \frac{1}{2\pi}\int_0^{2\pi} dx\, Q_{jk}(x)\, e^{-\mathrm{i}mx}\,. \tag{6}$$

Next, we assume statistical independence of the phases and the corresponding Fourier coefficients. We expect this independence to be valid for a large population, where many different couplings influence each phase. This assumption

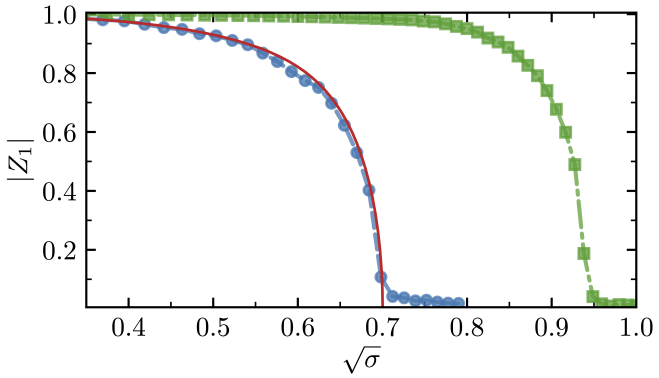

Рис. 1: Behavior of the first order parameter $\langle |Z_1| \rangle$ an ensemble of $N = 12 \times 10^3$ noisy rotators (1) with equal natural frequencies ($\omega_k = \Omega$) and coupling function $F(x) = K\big(\sin(x) + 4\sin(2x)\big)$ with $K = 1$ in dependence on $\sqrt{\sigma}$ for the moment of inertia $\mu = 0.5$. Green squares and blue circles are simulations without and with phase shifts, respectively. We consider random phase shifts α_{jk} distributed according to $G(\alpha) = (1 + \cos M\alpha)/2\pi$ with $M = 1$. Thus, the effective coupling function is $\mathcal{F}(x) = 0.5\,K\sin(x)$. For such coupling, the analytical expression (solid red line) for the order parameter in dependence on the noise intensity σ^2 can be written in the parametric (parameter R) form: $|Z_1| = 2\pi R I_0^2(R) I_1(R) \big/ \big(2\pi R I_0^2(R) + \mu K I_1(R)\big)$, $\sigma^2 = K|Z_1|/2R$, where $I_0(R)$ and $I_1(R)$ are the principal branches of the modified Bessel functions of the first kind with orders 0 and 1, respectively.

allows us to obtain the reduced coupling terms and conclude that the interaction is described with an effective deterministic coupling. For the Kuramoto-Daido-type model, we arrive at the effective averaged coupling function, Fourier modes of which are just $\langle f_{m,jk} \rangle$:

$$\frac{1}{N}\sum_{j=1}^{N} F_{jk}(\varphi_j - \varphi_k) \;\Rightarrow\; \frac{1}{N}\sum_{j=1}^{N} \mathcal{F}(\varphi_j - \varphi_k) = \frac{1}{N}\sum_{j=1}^{N} \langle F_{jk}(\varphi_j - \varphi_k) \rangle = \sum_{m} \langle f_{m,jk} \rangle\, e^{-\mathrm{i}m\varphi_k} Z_m. \tag{7}$$

For the random Winfree-type model, we have

$$\frac{1}{N}\sum_{j=1}^{N} S_{jk}(\varphi_k) Q_{jk}(\varphi_j) \;\Rightarrow\; \mathcal{S}(\varphi_k)\frac{1}{N}\sum_{j} \mathcal{Q}(\varphi_j) = \langle S_{jk}(\varphi_k) \rangle \frac{1}{N}\sum_{j=1}^{N} \langle Q_{jk}(\varphi_j) \rangle = \sum_{m} \langle s_{m,jk} \rangle\, e^{\mathrm{i}m\varphi_k} \sum_{m'} \langle q_{m',jk} \rangle\, Z_{m'} \,. \tag{8}$$

It is worth mentioning that because the Fourier transform is a linear operation, averaging the Fourier coefficients is the same as averaging the functions. Thus, our main theoretical result is that one can reduce the dynamics of a large population with random coupling functions to an effective ensemble without disorder, where the effective coupling functions are averages of the original random coupling functions.

The relations (7) and (8) are derived in the case of general randomness of interactions, which includes a situation where different coupling functions have different shapes. For example, some oscillators can be coupled via the first harmonic coupling function, while others are coupled with the second harmonic coupling function. A particular situation is one where all the shapes are the same, but the interactions differ in their coupling strengths and the phase shifts. Using (7) and (8) in the case where the randomness is restricted to coupling strength and phase shifts, one can see that the randomness of coupling strengths renormalizes the total coupling strength, but does not influence the shape of the coupling function. In contradistinction, the randomness of the phase shifts changes the form of the coupling function and the effective coupling function is the convolution operator of the original one with the phase shift distribution density. Our exhaustive numerical simulations confirm this theoretical prediction (e.g., see Fig. 1).

Summarizing the results, we have considered different models of globally coupled phase oscillators and rotators. In the case of a "maximal disorder", all the coupling functions are distinct and random, sampled from some distribution. Based on the assumption of independence of the phases and the coupling functions in the thermodynamic limit, we derived the averaged equations for the phases, where effective deterministic coupling functions enter. A more detailed consideration was devoted to the case where the shapes of the random coupling functions are the same, but the amplitudes and the phase shifts are random. Then, the effective functions are renormalized convolutions of the original coupling functions and the distribution densities of the phase shifts. In particular, if the distribution of the phase shifts possesses just one Fourier mode, the effective coupling function will possess only this mode, too. This property allows us to check the validity of the approach numerically because, for the one-mode coupling function, there are theoretical predictions for the behavior of the order parameters.

L.A.S. acknowledges support from the RSF (grant no. 22-12-00348).

Universality and scale-to-scale information flow in turbulence

Osaka University, Tomohiro Tanogami

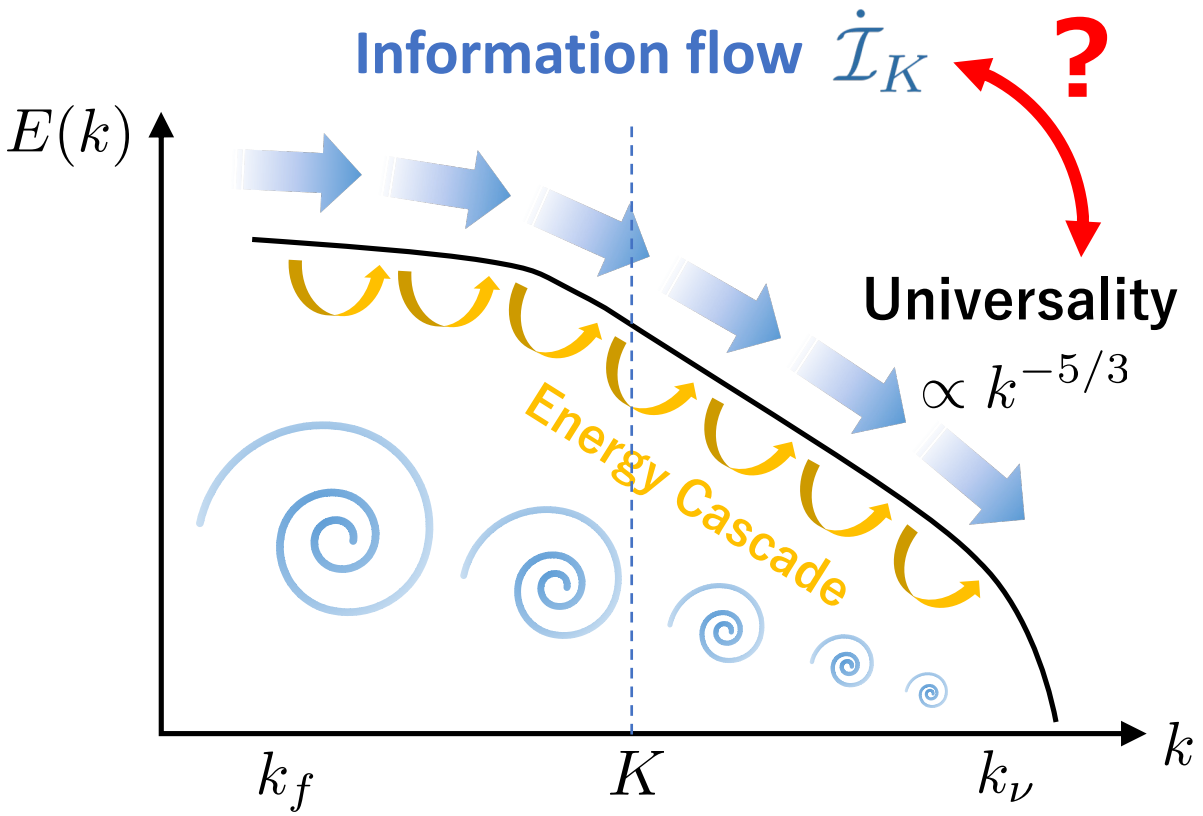

Result 1: Direction of information flow

Information flows from macro to micro

$$\dot{\mathcal{I}}_K \geq 0$$

Result 2: Scale locality

Information is propagated like a telephone game

$$\dot{\mathcal{I}}_K \simeq \dot{\mathcal{I}}_K^{\mathrm{local}}$$

Result 3: Information flow vs fluctuations

Information flow enhances turbulent fluctuations

$$\dot{\mathcal{I}}_K \leq C_p K \langle |u_{n_K}|^p \rangle^{1/p} \quad \text{for} \quad p \geq 1$$

Dynamical ergodicity breaking and scaling relations for finite-time first-order phase transition

Yu-Xin Wu[1], Jin-Fu Chen[1,2,*], and H. T. Quan[1,3,4,†]

[1]School of Physics, Peking University, Beijing, 100871, China

[2]Instituut-Lorentz, Universiteit Leiden, P.O. Box 9506, 2300 RA Leiden, The Netherlands

[3]Collaborative Innovation Center of Quantum Matter, Beijing, 100871, China

[4]Frontiers Science Center for Nano-Optoelectronics, Peking University, Beijing 100871, China

E-mail: yuxinw@stu.pku.edu.cn, jinfuchen@lorentz.leidenuniv.nl,, htquan@pku.edu.cn

Abstract

Hysteresis and metastable states are typical features associated with ergodicity breaking in the first-order phase transition which occurs in the thermodynamics limit. When the system is quenched across a first-order phase transition, the excess work (enclosed area between the dynamic and static hysteresis) even exhibits universal scaling behavior. Nevertheless, for a system of finite size, how will the features of the first-order phase transitions persist remains unexplored. We study the scaling behavior of the excess work as a function of the quench rate in the Curie-Weiss model. We find the shrinking of the hysteresis when downsizing the system, and the crossover of the scaling of the excess work from $v^{2/3}$ to v. Our study elucidates the interplay between the quench rate and the relaxation rate (system size), which leads to the dynamical ergodicity breaking and different scaling behavior of the excess work.

1D mean-field Curie-Weiss model

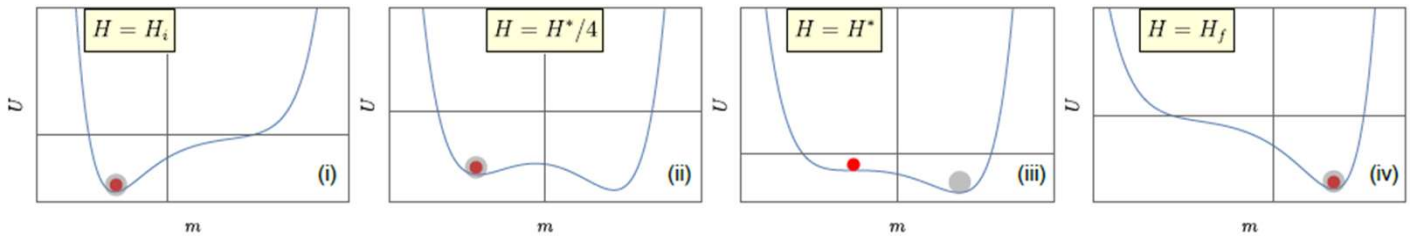

1. Infinitely large system

- Deterministic equation of motion

$$\frac{dm}{dt} = \frac{2}{\tau_0}\Big[\sinh(\beta J m + \beta H) - m\cosh(\beta J m + \beta H)\Big]$$

- We consider a linear protocol

$$H(t) = H_i + (H_f - H_i)\frac{t}{t_f},$$

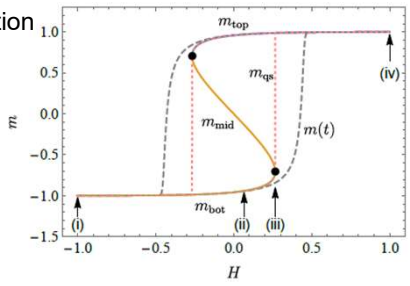

- Expand the EMO around the turning point for small quench rate

$$\frac{d\hat{m}}{d\hat{t}} \approx \frac{2}{\tau_0}\left[\beta J\sqrt{\beta J - 1}\hat{m}^2 + \sqrt{\frac{\beta}{J}}v\hat{t}\right].$$

- $v^{-1/3}$ scaling relation of the delay time and transition time

$$\hat{t}_{\rm del} = -A_1'\left[4\sqrt{\beta J(\beta J-1)}\frac{\beta}{\tau_0^2}v\right]^{-1/3},$$

$$\hat{t}_{\rm trans} = -A_1\left[4\sqrt{\beta J(\beta J-1)}\frac{\beta}{\tau_0^2}v\right]^{-1/3},$$

where $A_1' \approx -1.019$ and $A_1 \approx -2.338$ are zeros of Airy functions.

- $v^{2/3}$ scaling relation of the excess work

$$w_{\rm ex} \approx \frac{-A_1(1+\sqrt{1-\frac{1}{\beta J}})}{\left[4\sqrt{\beta J(\beta J-1)}\frac{\beta}{\tau_0^2}\right]^{1/3}}v^{2/3}.$$

2. Finite-size system

- Stochastic equation of motion

$$\frac{\partial P(M,t)}{\partial t} = \sum_{\eta=\pm}\Big[W_\eta(M_{-\eta},H(t))P(M_{-\eta},t) - W_\eta(M,H(t))P(M,t)\Big].$$

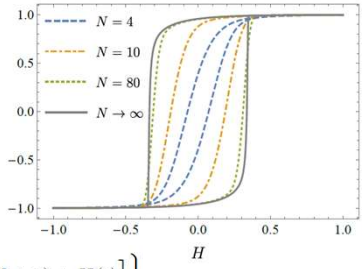

The transition rates under the external field H are given by

$$W_\pm(M,H(t)) = \frac{N \mp M}{2\tau_0}\exp\left\{\pm\beta\left[\frac{J}{N}(M \pm 1) + H(t)\right]\right\},$$

obeying the detailed balance condition.

- The average work can be computed from

$$\langle w\rangle = -v\int_0^{t_f} dt\langle m(t)\rangle.$$

- The average excess work is defined through $\langle w_{ex}\rangle = \langle w\rangle - w_{qs}$.

Table I. The scaling relation of the excess work $w_{\rm ex}$ with the quench rate v for different situations.

Finite-time isothermal process [34–39]	$w_{\rm ex} \propto v$
Finite-time adiabatic process [40–45]	$w_{\rm ex} \propto v^2$
Finite-time first-order phase transition[63–69]	$w_{\rm ex} \propto v^{2/3}$
Finite-time second-order phase transition [22, 46]	$w_{\rm ex} \propto v^{\delta_1}$

◆ **Crossover in the scaling relation from $v^{2/3}$ to v in finite N system**

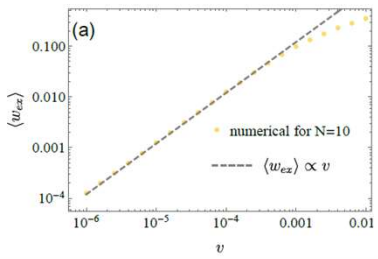

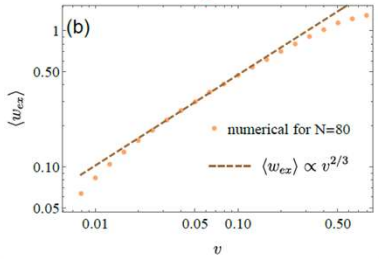

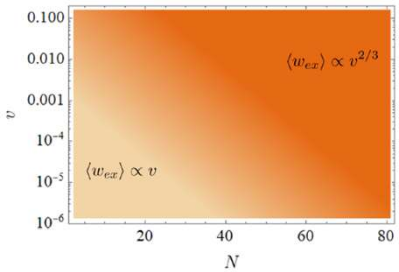

Reference Y. X. Wu, J. F. Chen and H. T. Quan, arXiv:2401.15592 (2024).

Phase coexistence in a weakly stochastic reaction-diffusion system

Yusuke Yanagisawa and Shin-ichi Sasa (*Dept. of Phys., Kyoto Univ.*)

Ref) arXiv.2403.19198

- **Research topic** : Phase coexistence in a reaction-diffusion system
  - ✓ Macroscopic system → deterministic and continuum description
  - ✓ Mesoscopic system → fluctuation effect
- **Model** : A stochastic reaction-diffusion system
  - ✓ coupled reaction vessels
  - ✓ bistable chemical reaction

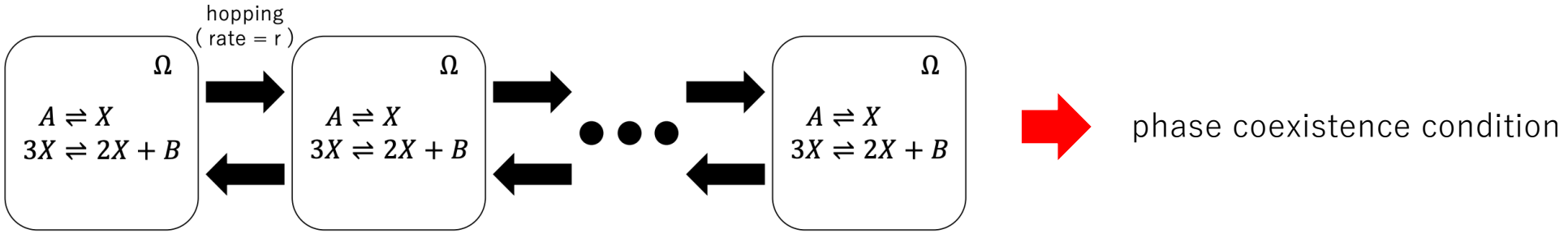

Phase coexistence in a weakly stochastic reaction-diffusion system

Yusuke Yanagisawa and Shin-ichi Sasa (*Dept. of Phys., Kyoto Univ.*)

Ref) arXiv.2403.19198

➢ Results

Phase coexistence condition

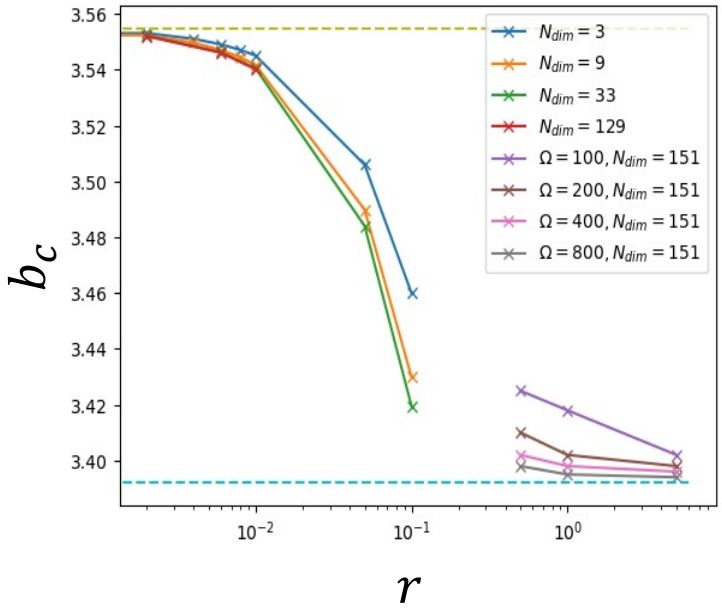

Phase coexistence condition for different regimes

✓ High-hopping-rate regime :
equivalent to the reaction-diffusion equation

✓ Low-hopping-rate regime :
NOT equivalent to the reaction-diffusion equation

Details will be explained in the poster !